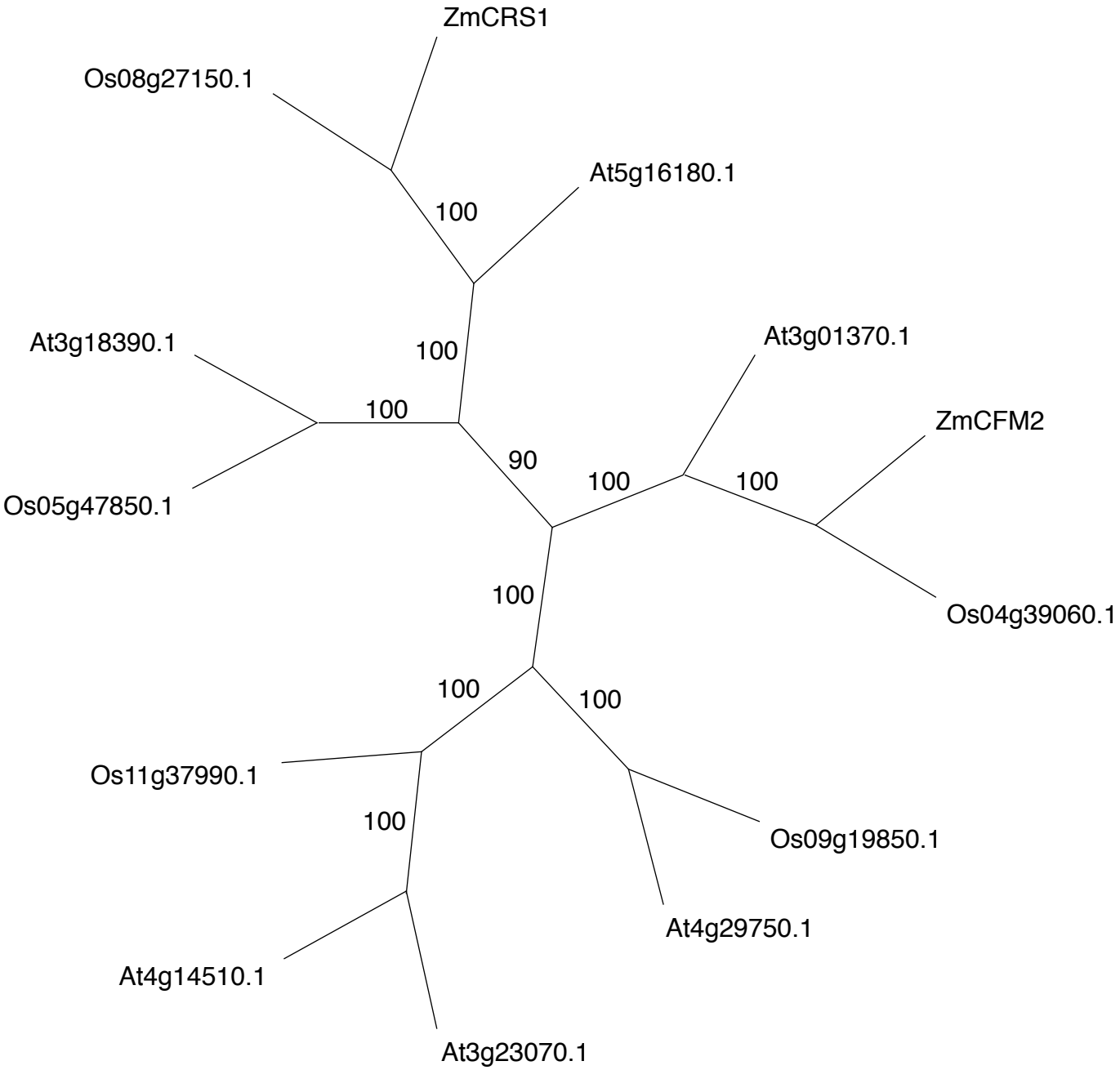

Supplemental Figure 1. Unrooted tree demonstrating orthology among maize, rice, and *Arabidopsis* CFM2.

A phylogenetic tree that includes the complete CRM protein families from rice and Arabidopsis was reported previously (Barkan et al, 2007) and defines the CRS1 subfamily. To generate the tree shown here, all CRS1 subfamily members from rice (Os) and Arabidopsis (At), and the characterized members of the subfamily from maize (Zm) were aligned in Clustal X. An unrooted tree was generated in PAUP 4.0, using the neighbor-joining method with 1000 bootstrap replicates.

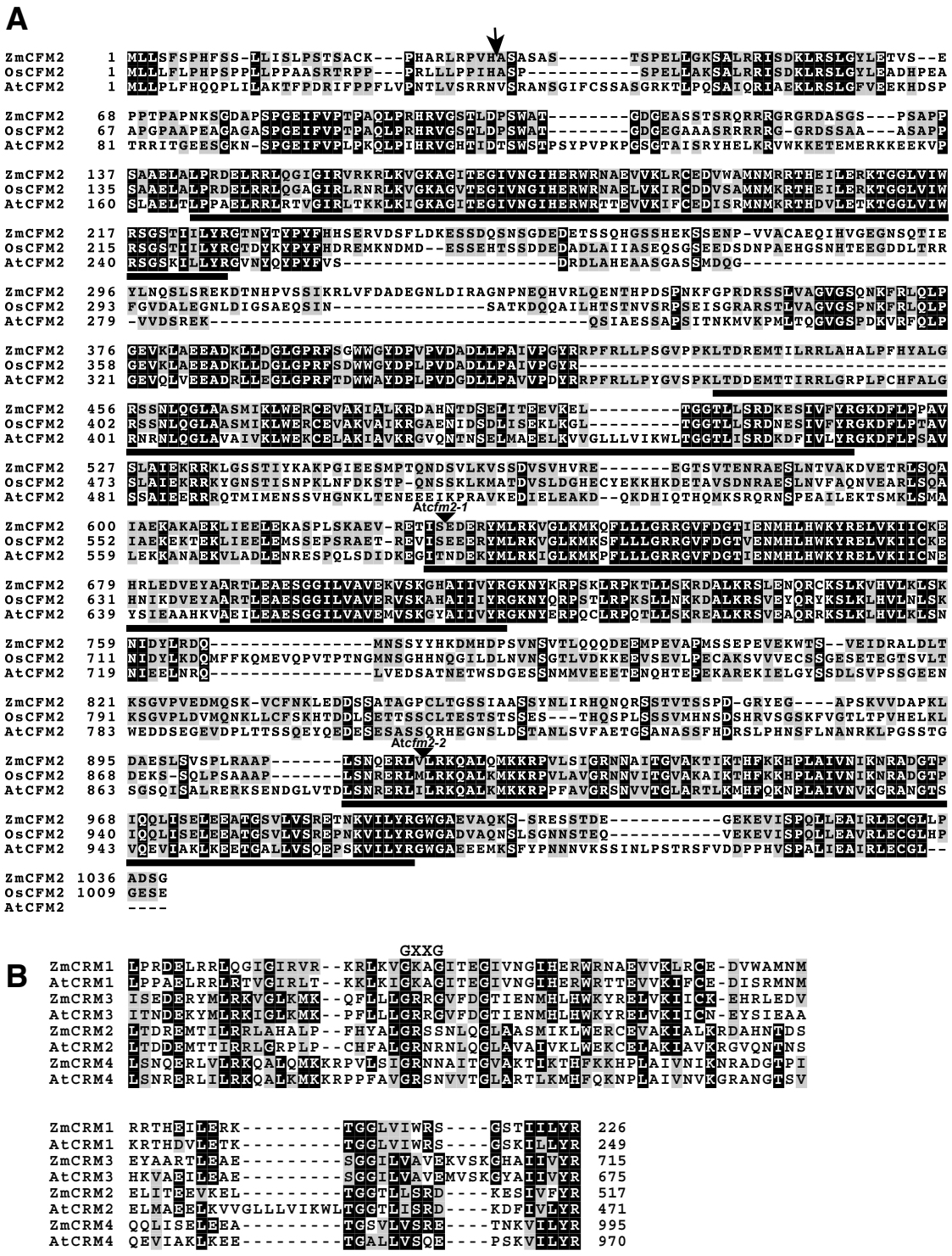

Supplemental Figure 2. Multiple sequence alignments of CFM2 proteins and CRM domains. The alignments were generated in ClustalW and shaded with BoxShade. Identical residues are shaded in black and similar residues in gray. **(A)** Alignment of AtCFM2, OsCFM2, and ZmCFM2. The predicted transit-peptide cleavage site in ZmCFM2 is indicated by the arrow. The positions of the T-DNA insertions in the Arabidopsis mutants analyzed here are indicated with triangles. The CRM domains are underlined. We believe this rice gene model (from TIGR) is erroneous as it is not supported by cDNAs and use of alternative splice junctions improves colinearity with the maize and Arabidopsis proteins. **(B)** Alignment of the CRM domains in AtCFM2 and ZmCFM2. The residues corresponding to the "GxxG" loop proposed to contribute to RNA binding (Barkan et al, 2007; Ostheimer et al, 2002) are indicated.

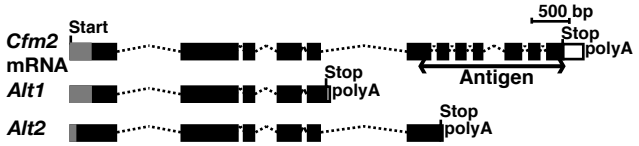

Supplemental Figure 3. Maize cfm2 cDNA variants.
Exons are indicated with boxes and introns with dotted ines. The gray exon segments at the 5' ends were inferred from genomic DNA sequence and encode the start codon. The top diagram shows the cDNA encoding the full-length protein, which is best conserved with the predicted rice and Arabidopsis orthologs and is shown in Supplemental Figure 2. Two mRNA variants resulting from the use of alternative polyadenylation sites were detected as cDNAs and are diagrammed below. Alt1 and Alt2 encode proteins ending within and after the third CRM domain, respectively. These RNAs were not detected by RNA gel blot hybridization of seedling leaf RNA; the cDNAs may be derived from non-leaf tissues that contributed to the mixed tissue cDNA library. The smaller protein detected in leaf by CFM2 antisera is not derived from these alternative mRNAs because the Alt1 form lacks sequences encoding the antigen, and affinity purification of the sera against a peptide that is not encoded by Alt2, which in any case overlapped the antigen only slightly, did not change the ratio of the two bands detected.

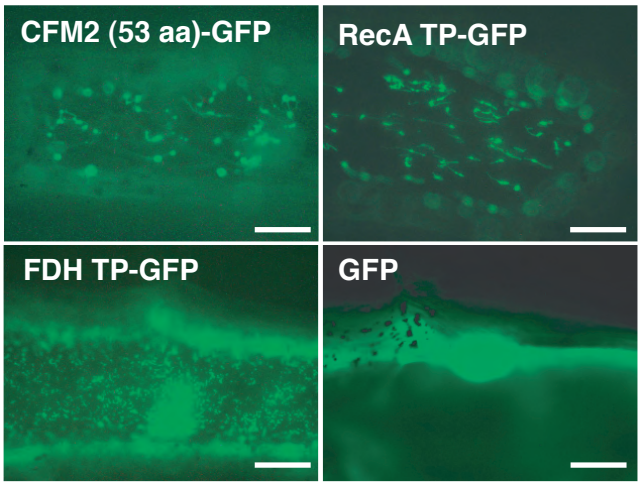

Supplemental Figure 4. Chloroplast localization of CFM2-GFP in onion epidermal cells.
A fusion protein consisting of the N-terminal 53 amino acids of maize CFM2 fused at their C-terminus to GFP was transiently expressed in onion root epidermal cells. GFP fused to the transit peptides of chloroplast RecA and mitochondrial FDH were used to visualize chloroplasts and mitochondria, respectively. The panel labeled GFP shows results of transformation with pOL-LT, the vector encoding GFP alone. Bars =5 μm.

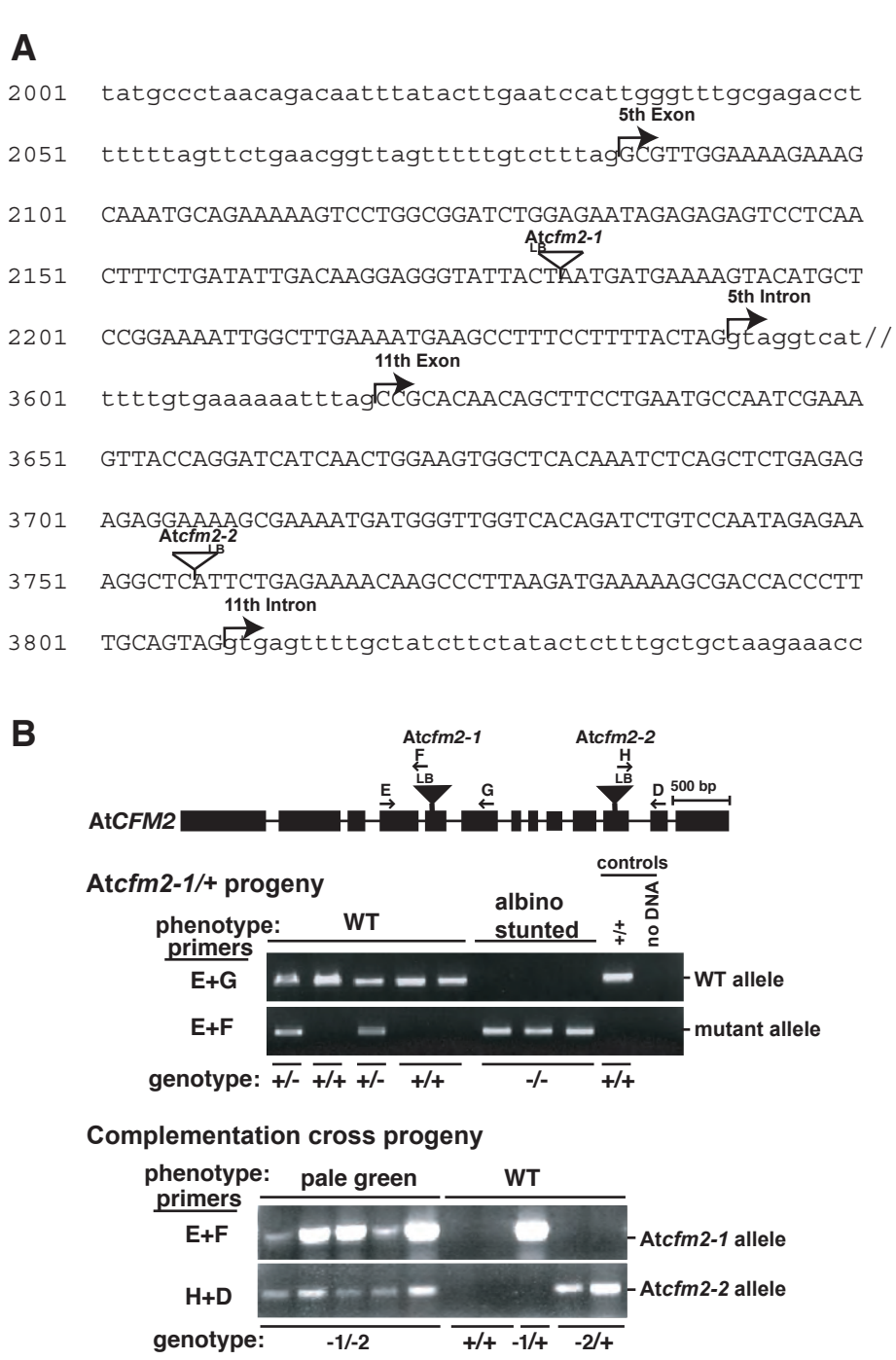

Supplemental Figure 5. T-DNA insertions in At*CFM2*

(A) T-DNA insertion sites. Nucleotide residues are numbered according to the distance from the beginning of the open reading frame in the genomic sequence. Insertion sites were determined by sequencing PCR fragments resulting from amplification with a primer for the T-DNA left border (LB) and the gene specific primers shown in panel (B).

(B) Linkage between seedling phenotypes and At*CFM2* mutations. The primers used for PCR-genotyping are diagrammed in the map. The middle panel shows the genotypes of normal (WT) and albino stunted seedlings segregating in the progeny of At*cfm2-1* plants. The albino stunted seedlings germinated from shriveled seeds, whereas the normal seedlings germinated from seeds of normal morphology. Only a fraction of the shriveled seeds germinated. The bottom panel shows the genotypes of the progeny of allelism crosses. DNA from pale green (mutant) and normal (WT) progeny of a cross between At*cfm2-1*/+ and At*cfm2-2*/+ plants was analyzed by PCR. The deduced At*CFM2* genotype is shown below. All of the pale green progeny harbored both mutant alleles, whereas none of the green progeny did, confirming that the insertions in At*CFM2* are responsible for the chlorophyll-deficient phenotype.

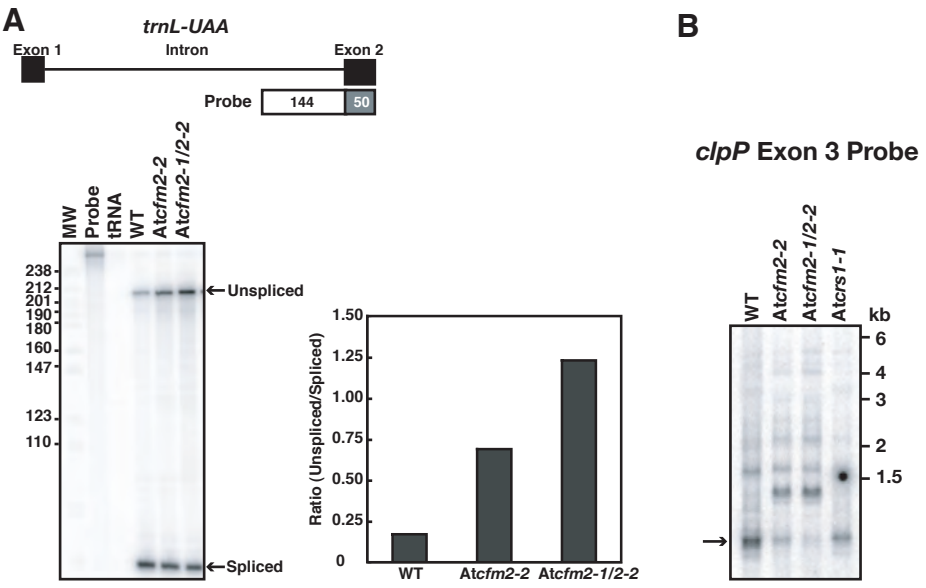

Supplemental Figure 6. Confirmation of splicing defects in At*CFM2* mutants.
(A) Ribonuclease protection assay of *trnL-UAA* splicing in At*CFM2* mutants. The radiolabeled probe spanned the 3' splice junction, as diagrammed at the top, and included vector-derived sequences that were digested during the assays. The ratios of unspliced to spliced RNAs were quantified with a phosphorimager, and are plotted in the bar graph.
(B) RNA gel blot hybridization showing loss of fully spliced *clpP* mRNA, indicated with an arrow.

Supplemental Table 1. Top-Ranking Fragments in CFM2 RIP-Chip Assays

		αCFM2		Control		
Fragment name	Fragment Number[a]	Median Log_2 Ratio[b]	*n*[b]	Median Log_2 Ratio[b]	*n*[b]	P Value[c]
trnL-UAA2	88	1.4	20	-4.2	10	4.5E-13
ycf3int1ex1	80	1.3	20	-2.3	10	1.4E-12
ycf3ex2int1	79	1.3	20	-3.0	10	3.8E-10
trnL-UAAint/ex2	89	0.5	15	-4.5	8	5.1E-04
ndhAint	243	-0.2	20	-3.4	10	3.9E-14
ycf3ex1/trnS5'	81	-0.4	20	-2.9	9	6.4E-10
ndhAintex1	244	-0.6	20	-3.3	10	1.0E-12
ycf3int2	78	-0.6	16	-3.4	10	1.8E-07
ndhAex2int	242	-1.3	20	-3.3	10	1.6E-04
ycf3int2ex3	77	-1.6	20	-3.4	10	8.3E-11
ndhBintron	185	-2.1	20	-3.6	9	2.4E-06
rrn16-3prime	200	-2.1	18	-1.8	9	4.4E-01
trnS-GGA1	82	-2.3	12	-3.9	8	1.1E-06
rrn16/trnIint	201	-2.4	12	-2.8	8	5.6E-01
rps12int2ex2	191	-2.4	20	-2.8	9	9.7E-03
rps12int13'	194	-2.5	20	-3.2	10	1.2E-01
trnI-GAUcomplete	203	-2.5	20	-2.3	10	6.3E-01
trnA-UGCcomplete	206	-2.5	12	-2.4	6	7.7E-01
ndhBint2	186	-2.6	12	-3.8	6	9.0E-04
trnI/trnA	205	-2.7	20	-2.0	10	4.7E-02
trnA-int	207	-2.8	20	-2.3	10	1.9E-02
rps12int2A	190	-2.8	20	-3.5	8	4.1E-02
ndhBex2int	184	-2.8	20	-2.8	9	7.2E-02
rps12ex2int13'	193	-2.8	20	-3.8	10	3.8E-03
ndhI/ndhA	241	-2.8	20	-3.6	10	2.8E-03
orf139	176	-3.0	20	-2.0	10	8.7E-03
ndhBex1	187	-3.0	17	-3.7	10	2.1E-02
rps7/rps12ex3	189	-3.0	20	-3.1	10	3.6E-01
trnI-GAUex1/int	202	-3.0	19	-3.2	10	6.0E-01
trnA-UGC/23S5'	209	-3.0	20	-2.6	10	1.7E-03
rps12int2B	192	-3.1	20	-3.4	10	1.2E-01
rpl2ex2int	167	-3.1	20	-3.7	10	6.3E-02
psaC/ndhE/ndhG	236	-3.1	16	-2.2	10	2.9E-02
rps4	84	-3.1	20	-2.4	10	2.3E-01
rpl2int/ex1	169	-3.1	20	-3.3	10	8.7E-02
trnS/rps4	83	-3.2	8	-3.7	8	1.9E-02
trnV-UACex2int	97	-3.2	19	-3.4	8	6.8E-01

Elements ranking in the top 15 % for median normalized enrichment ratio in four replicate assays with CFM2 antibodies are ordered according to the magnitude of their enrichment.

[a]Fragments on the array are numbered according to chromosomal position. The nucleotide residues on each fragment are described in Array Express (accession number A-MEXP-743) and in Schimitz-Linneweber et al. (2005).

[b]Median (log_2F635/F532) normalized across experiments with αCFM2 and control (αOE16 and αOE23). Replicate experiments constitute a total of *n* replicate spots.

[c]P values were calculated with a *t* test (two-tailed, unequal variance) and represent the probability that there is no difference in enrichment between the αCFM2 and control immunoprecipitations.